A Human Vision Based Computational Model for Chromatic Texture Segregation

Thomas V. Papathomas, *Member, IEEE*, Ramanujan S. Kashi, and Andrei Gorea

***Abstract*—We have developed a computational model for texture perception which has physiological relevance and correlates well with human performance. The model attempts to simulate the visual processing characteristics by incorporating mechanisms tuned to detect luminance-polarity, orientation, spatial frequency and color, which are characteristic features of any textural image. We obtained a very good correlation between the model's simulation results and data from psychophysical experiments with a systematically selected set of visual stimuli with texture patterns defined by spatial variations in color, luminance, and orientation. In addition, the model predicts correctly texture segregation performance with key benchmarks and natural textures. This represents a first effort to incorporate chromatic signals in texture segregation models of psychophysical relevance, most of which have treated grey-level images so far. Another novel feature of the model is the extension of the concept of spatial double opponency to domains beyond color, such as orientation and spatial frequency. The model has potential applications in the areas of image processing, machine vision and pattern recognition, and scientific visualization.**

I. Background and Significance

TEXTURE perception is a very important task for early visual information processing and it has been receiving increasing attention in recent years. In psychophysics, systematic work on texture began rather late [3], [32], [33], as compared to work on other low-level visual processes, such as color, motion, and stereo. Computational modeling efforts in texture also lagged behind those in motion or in stereopsis (for a critical survey see Bergen [6]). Julesz [32] pioneered a quantitative approach, based on the statistical properties of the texture images. His conjecture that textures with identical first- and second-order correlation functions do not segregate [35] was eventually disproved [36]; nevertheless, it motivated further quantitative work and pointed to the importance of local differences. Beck's conceptual model [4], [5] relied on feature detectors and "similarity grouping," but lacked a computational implementation. Quantitative attempts at modeling began with textures formed by sums of sinusoidal gratings [29], [47], in an effort to relate texture discrimination to differences in activity of channels that possess only spatial frequency selectivity.

With respect to relevance with biological vision, automated texture segregation efforts have resulted in two broad categories: human-vision-related and "pure" machine vision texture segregation models. In the first belong models that are designed to produce results that correlate well with human performance, when tested with the same classes of stimuli. Typically, the structure, signal pathways, and processing stages of models in this category are based on neurophysiological correspondences (see Bergen [6]). The algorithms and models in the second category perform texture segregation on input images without necessarily employing neurophysiological principles. More often than not, such models do not attempt to duplicate human performance because there are no apparent advantages for such correlation. Caelli [14]–[15] provides a comprehensive review for this class of models. The model presented in this paper belongs to the first category. Accordingly, in the rest of the paper the problems are discussed mainly from the human vision point of view. Nevertheless, by extending the concept of double opponency, the model introduces a new research direction in both categories, machine and human visual texture modeling.

In what follows, we give a brief but comprehensive survey of earlier models. Since the only major extension of our model is to process the chromatic signal, in addition to the luminance signal that most early models deal with, we do not attempt a critical analysis of existing models. Caelli [12] developed filters that were tuned to orientation and to spatial frequencies, and used them to predict texture discrimination performances. Caelli's [13] model set the trend for a wide class of later models and uses three stages. i) Convolution by oriented filters, which essentially model the response properties of cells in mammalian striate cortex; this is followed by one or more nonlinear operations. ii) "Impletion," to spread of activity of similar proximal filters (the term "spatial pooling" is currently used in the literature). iii) Grouping, to locate texture boundaries, by attempting to maximize the correlation between activity levels within regions and minimize it between regions. Zucker [62] studied the interactions of the outputs of simple-cell-like filters in spatially varying oriented textures and applied a minimization scheme to obtain segmentation. A neural network approach was developed by Grossberg and Mingolla [28]. In the line of Caelli's approach, Turner [56] uses a bank of Gabor filters to a variety of pre-attentively discriminable textures and shows that the differently textured regions are distinguished by first-order differences in the values measured by the filters.

Manuscript received March 18, 1995; revised March 19, 1996. This work was supported by the National Science Foundation under Grant BNS-9109384 and the Theodore N. Garbis Research Fund of the Fight for Sight Research Division of Prevent Blindness America.

T. V. Papathomas is with the Laboratory of Vision Research and Department of Biomedical Engineering, Rutgers University, Piscataway, NJ 08854 USA (e-mail: papathom@zeus.rutgers.edu).

R. S. Kashi is with Bell Laboratories, Murray Hill, NJ 07974 USA.

A. Gorea is with the Laboratoire de Psychologie Expérimentale, Université René Descartes and Centre National de la Recerche Scientifique, 75006 Paris, France.

Publisher Item Identifier S 1083-4419(97)02920-8.

In the last few years, several complex models have been developed, some of which address directly the issue of neurophysiological relevance, and most attempt to achieve close agreement with results from psychophysical experiments. Bergen and Adelson [7]–[8] use the local energy of linear oriented filters at various scales to account for scale invariance in texture segmentation, and achieve close agreement with human performance. Good fits are also achieved by Sagi and his colleagues, who use a similar energy approach [22], [47]–[48]. Sperling [51] differentiates between first-order linear (Fourier) and second-order nonlinear (non-Fourier) rectifying regimes. He makes an analogy between an object's texture and the carrier in amplitude modulated (AM) communication. The same analogy is made by Clark, Bovik, and Geisler [18], who use the spatially pooled amplitude and phase responses of Gabor filters; they recognize that their implementation offers primarily a machine vision method, as does that of Voorhees and Poggio [60]. Sutter, Beck, and Graham [52] examine the discrepancies between data and their linear-filter model predictions to arrive at two possible nonlinearities [26], [27], which improve the fit substantially. Malik and Perona [40] model human pre-attentive texture perception in three stages which have close parallels with Caelli's [13] model. i) Convolution of the image with a bank of orientation- and frequency-tuned filters, followed by half-wave rectification, to "model outputs of V1 simple cells." ii) Inhibition, localized in space within and among the responses, to suppress spurious responses in the presence of stronger ones. iii) Spatial pooling and texture edge extraction by odd-symmetric mechanisms. They obtained close fits with experimental data. Landy and Bergen [9], [38] use multi-scale oriented energy computations, followed by spatial pooling. They match closely observers' performance by introducing the idea of opponency to the attribute of orientation. This opponency is similar to a co-extensive single-opponency found in the ganglion and geniculate neurons for the chromatic attribute. Finally, an elegant approach in texture perception is the "orthogonal distribution analysis" of Chubb and Landy [17], which has the potential of estimating the parameters of texture segregation models.

Almost all of the biological vision models accept a grey-level texture image as input, i.e., they work exclusively in the luminance domain. As a result, they concentrate on differences in the figural, or form, features of the texture elements (textels), while all other attributes of the textels (luminance, color, stereo disparity, etc.) remain fixed. The model presented here works well with stimuli in which textels are defined by combinations of three attributes, i.e., color, luminance, and orientation. Its design is based on experiments which enabled us to study the *interaction* of several attributes in the texture segregation process [24].

One of the advantages of the double-opponency model of this paper is the incorporation of chromatic signal processing mechanisms for texture segregation in color images. The idea of double-opponency is explained in Section II-A4. The second major development in the model is the extension of the idea of double-opponency to other attributes, in addition to color, which introduces a new research direction in modeling. We believe it worth pursuing not only because of the respectable fit to the data in the study, but also because there is psychophysical [16], [45], [49] and neurophysiological [10], [37], [58], [59] evidence supporting spatial opponency (not necessarily double) in attributes other than luminance or color. It is widely accepted that the human visual system has three opponent mechanisms which represent the perceptual color space: 1) bright-dark (broad band) opponency, 2) red-green opponency, 3) red+green (yellow)-blue opponency. We have considered the first and second opponencies as a first step in including color for texture perception.

II. Modeling Strategy

The aim has been to develop a computational model which accepts texture images as input and predicts human performance in texture segregation. The model is implemented in five stages (see Fig. 1): i) Image decomposition into chromatic and achromatic (luminance) signal components. ii) Processing of the chromatic and luminance signals by separate parallel pathways. Within both the color and luminance pathways there exist two domains. One comprising isotropic and another comprising oriented linear filters tuned to specific spatial frequencies. iii) A set of nonlinear operators to eliminate spurious weak responses. iv) Double-opponent units to extract texture edges. v) Mechanisms that combine the outputs of the various domains. The last step is to compare the model's predictions with results from earlier experiments [25] and also to test the model's performance with key texture stimuli.

A. Model Description

We employed opponent mechanisms in a texture segregation model, the block diagram of which is schematized in Fig. 1. It is grossly oversimplified for clarity's sake. It shows filters that are broadly tuned only to one spatial frequency and two orientations. In the actual implementation, there were a bank of filters (horizontal, vertical, left diagonal and right diagonal) that span the orientation ranges [19]. The input to this computational model is, of course, the actual image viewed by observers in the experiments, so as to compare performances. The following assumptions were made in developing the model: 1) The image signal is composed of a luminance component $L(x, y)$ and a chromatic component $C(x, y)$, each being processed by separate pathways. This is a reasonable first-order approximation, supported by neurophysiological evidence [21], although there are some secondary interactions in the pathways [20], [50], [53]. In our implementation we have accounted for the secondary interactions by weighing the chromatic input by the luminance signal that is present at the same position (see Section II-A1). 2) Even-symmetric cells, but not odd-symmetric cells, contribute to texture segregation. A persuasive argument for this assumption is developed by Malik and Perona [40]. Suffice it to say here that the odd-symmetric cells may encode spatial phase [20], and phase does not seem important for texture segregation because texture, by its very nature, contains random phase signals. 3) There are four types of domains, labeled according to the populations of cells that they contain: Luminance-nonOriented

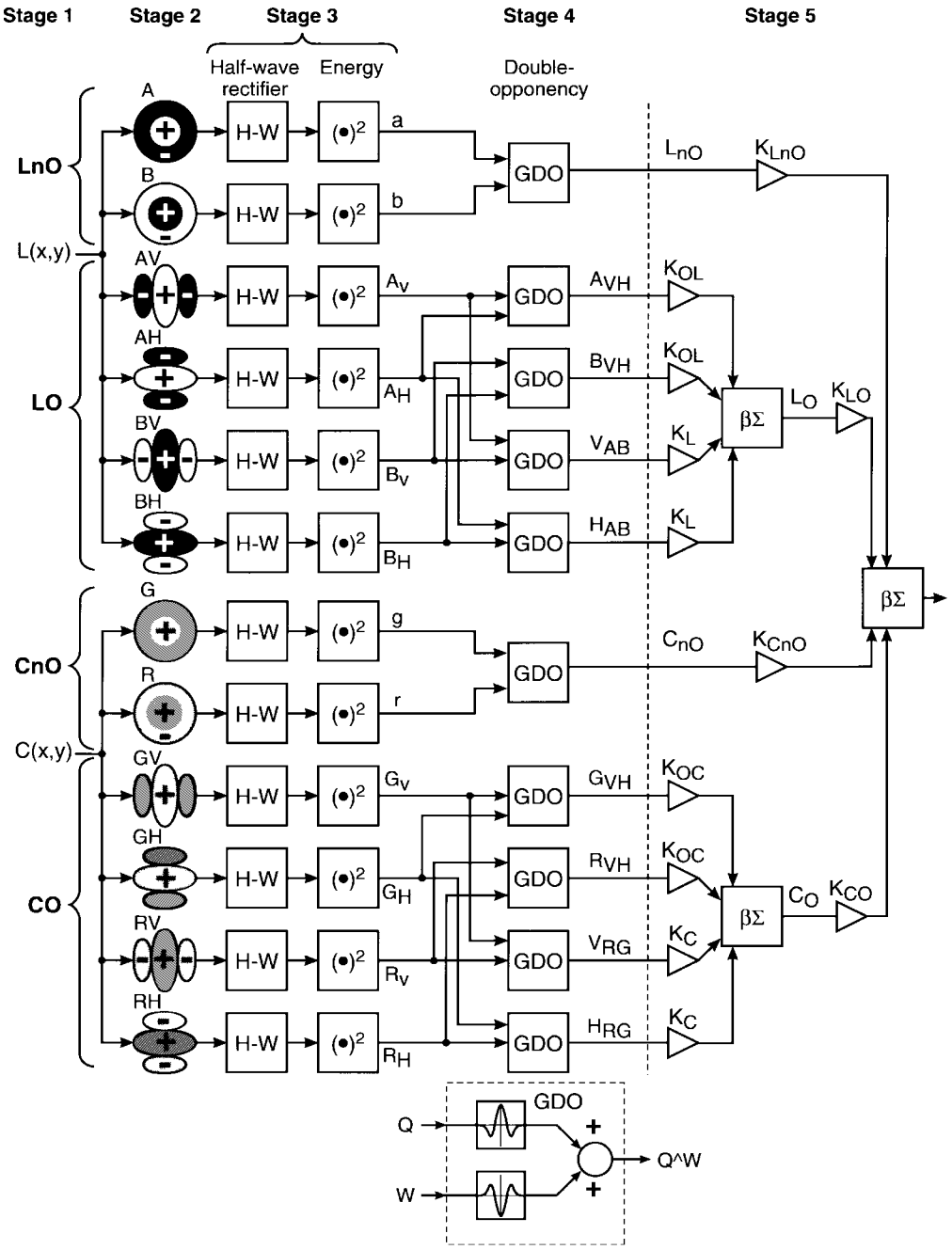

Fig. 1. Block diagram showing the five stages of the model for texture segregation. In the first stage, the input image is decomposed into chromatic, $C(x, y)$ and luminance, $L(x, y)$ components. The decomposed image is convolved in stage 2 with a set of oriented and non-oriented filters, and then, in stage 3, half-wave rectified and squared. The texture edges are computed across selected pairs of activity maps in stage 4, by convolving with double-opponent filter cell responses. Finally, in stage 5, the texture edges across pairs are combined through probability summation to obtain the final texture gradient.

(LnO), Luminance-Oriented (LO), Color-nonOriented (CnO), and Color-Oriented (CO). The first two types of domains are essentially color-blind and operate entirely in the achromatic domain. The last two types of domains are luminance-blind and care only about wavelengths, but are influenced to some degree by the luminance mechanisms at the same location. The LnO domain contains luminance driven spatial frequency-tuned isotropic filters of the opponent center/surround type; the center lobe of their respective field is excitatory, and the surrounding disk is inhibitory (center-ON) or vice versa (center-OFF). The LO domain comprises luminance-driven filters that are simultaneously tuned to orientation and spatial frequency. The CnO and CO domains contain similar opponent center/surround and oriented filters, respectively, that are color-driven. The first three domains (LnO, LO, and CnO) are well documented in the physiological literature [39], [54]; the evidence for color oriented cells is mostly psychophysical [11], [24], but there are similar findings in physiology as well [55].

The model has five major stages, and its architecture follows the archetypal structure of Caelli [13], which has been followed by most recent biological models. These stages are presented below in reference to Fig. 1. Our rationale is given

for our approach, whenever possible, and alternatives are examined.

1) Input Image Decomposition: Each input image was decomposed into two maps: The luminance and chromatic maps. Each pixel at location (x, y) in the original input image is characterized by two values $R(x, y)$ and $G(x, y)$, which represent the intensities of the red and green components, respectively; in our implementation; $0 \leq R, G \leq 127$. The luminance map was obtained from the input image by summing the red and green values at each point in the image $L(x, y) = R(x, y) + G(x, y)$. The chromatic map was obtained by finding the arc-tangent of the ratio of the green value to the red value at each point in the image $(C(x, y) = \tan^{-1}\{G(x, y)/R(x, y)\})$. This angle was linearly mapped to a scale between 0 and 255 where the values 0, 127, and 255 represent a pure red, a yellow and a pure green signal, respectively, i.e., a linear color scale representation. Thus, if we map R and G onto the horizontal and vertical axes, respectively, of a Cartesian coordinate system, then contours of constant L map on straight lines of slope $-45°$ with L increasing as we move away from the origin, and contours of constant C map on straight lines passing through the origin, following standard notational practice in color psychophysics. It is important for the color value to change linearly as we traverse from any point on the horizontal axis to a point on the vertical axis. This is achieved by making C a function of the angle that a point with coordinates (R, G) forms with the horizontal axis, and $\tan^{-1}(G/R)$ satisfies this criterion. The chromatic map was further modulated by a nonlinear function of the luminance at the same location. Among nonlinear functions with sigmoid profiles, we selected the inverse tangent function. This is needed to account for secondary interactions of luminance and chromatic pathways. The luminance map is supplied to the luminance oriented (LO) and non-oriented (LnO) mechanisms and the chromatic map is supplied to the chromatic oriented (CO) and non-oriented mechanisms (CnO) of the model.

2) Linear Mechanisms: The luminance $L(x, y)$ and color $C(x, y)$ signals are first convolved by linear filters, belonging in the four domains. In this stage we are essentially modeling the spatial processing characteristics of the early visual cortical areas. The LnO domain comprises the center ON (A in Fig. 1 stands as a mnemonic for "Above") and center-OFF (B for "Below" in Fig. 1) kernels. These are isotropic filters which model non-oriented opponent center-surround simple cells. The LO domain has the center-ON vertical (AV) and horizontal (AH) filters and the corresponding center-OFF (BV and BH) oriented filters. These directionally tuned filters, which have even-symmetric profiles, model the classical Hubel–Wiesel [31] type bar-sensitive detectors. The chromatic domains CnO and CO have corresponding kernels, with OFF and ON substituted by red (R) and green (G), respectively. The chromatic non-oriented filters model the concentric single-opponent filters. Filters tuned to other orientations (not shown here for simplicity) were used in the final model. The spatial frequency of these filters was chosen to match the stimuli used in the psychophysical experiments. Thus, our approach is similar to that of Fogel and Sagi [22],

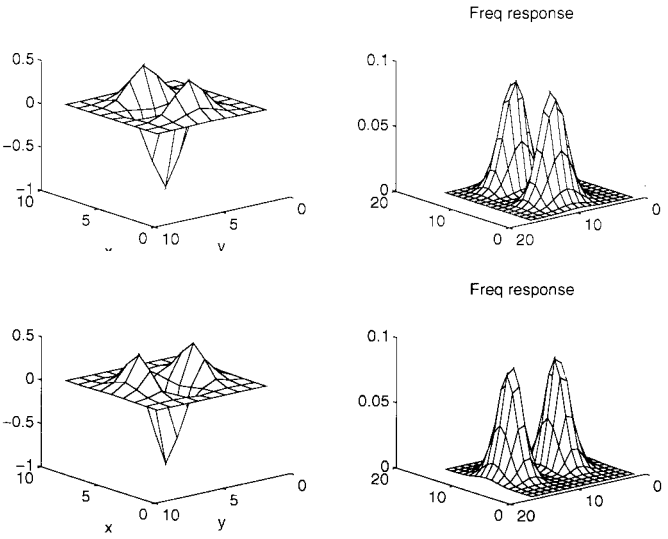

Fig. 2. Oriented filters shown with their frequency responses. These were designed by the steerable filters described in the text. The oriented filters, designed as second derivative of Gaussians, model units in the LO and CO domains. From the frequency responses, it can be noted that they are essentially band-pass filters.

i.e., to use the scale that provides the strongest texture edge; we experimented with smaller and larger scales and, as expected, the edge strength was significantly reduced relative to the near-optimal scale. These filters essentially model the point-spread function of simple cells and subunits of complex cells. The choice of filters is not very crucial. We have used the second derivative of Gaussians since they yield frequency and orientation bandwidths that are in reasonable agreement with physiological and psychophysical estimates.

We used "steerable filters" as described by Freeman and Adelson [23], to design our oriented filters. By this technique one can obtain the response of a filter of arbitrary orientation as a linear combination of the responses of a set of "basis filters." These basis filters were all x-y separable filters, which allowed steerable filters to be applied with high computational efficiency. In our case we used three x-y separable basis filters to design all the orientations. Two orientations of filters used and their corresponding frequency responses are shown in Fig. 2. However, with the same basis filters one could enhance the orientation selectivity by choosing an arbitrary number of orientations.

3) Nonlinear Mechanisms: The outputs of the linear filters are transformed with what Heeger [30] termed "half-squaring," i.e., they are first half-wave rectified and then squared. Simulation results with this kind of nonlinearity correlate well with a large body of neurophysiological data. Heeger [30] used this transformation for modeling units in the cat's visual cortex. In addition to being a good physiological model, half-squaring also makes sense for texture segregation. Let us consider a specific activity map, say the center-ON vertical (AV). Ideally, AV should produce a strong positive signal S when it is centered on a bright vertical textel (texture element). However, there will be negative values in the output at certain off-center locations. Half-wave rectification will conveniently eliminate these negative responses. At the same time, we must

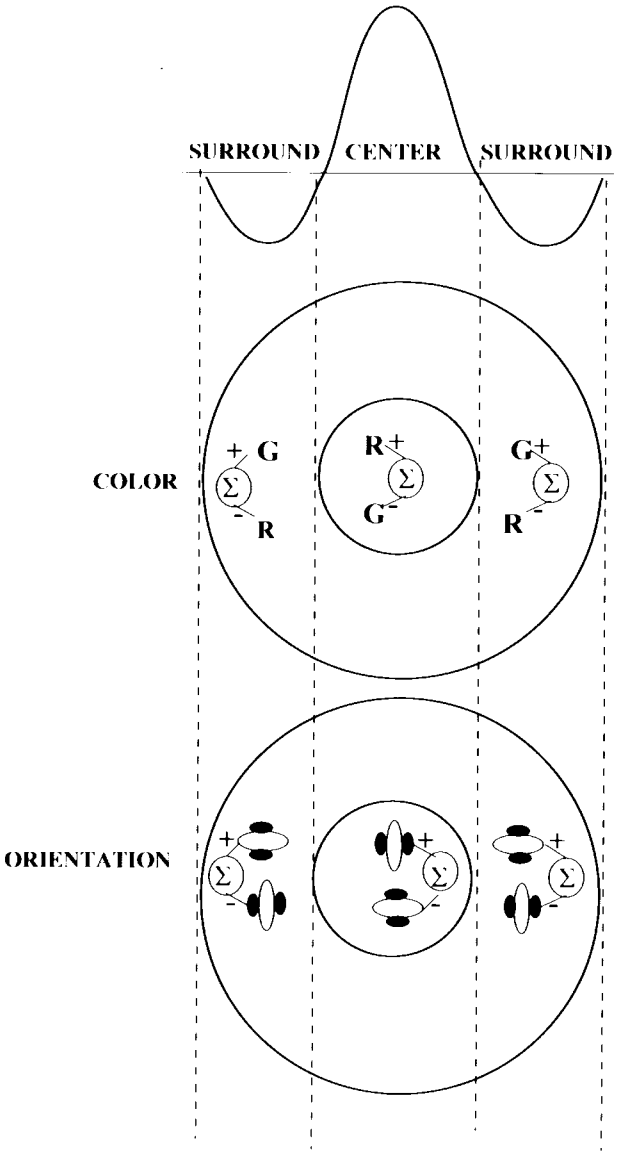

Fig. 3. Double opponency illustrated for color and orientation. In the color case there is chromatic opponency at the centers (R^+ and G^-) and surround (G^+ and R^-). The second opponency is of the spatial kind between the center and surround (R^+ and R^-; G^- and G^+). The orientation case is analogous to the chromatic case, with R replaced by vertical and G by horizontal.

minimize the undesired responses of the AV filter to a dark vertical textel. The strong negative response produced when such a textel is centered on the AV filter's receptive field is eliminated by half-wave rectification. However, the AV filter will also produce some weaker positive response, say s, for some off-center locations. Ideally, we would like the ratio S/s to be as large as possible. Squaring has a beneficial effect in that it enhances this ratio. Another way of increasing this ratio would be to use a nonlinear contrast response function g. Typically g has a sigmoidal shape with neurons that exhibit a threshold effect for low contrast and a saturation effect for high contrast [2].

Notice that after half-squaring, the units in each domain fire specifically for one polarity or one color and orientation. Thus the units in the CO domain are simultaneously tuned to color and orientation. For example the RV units fire for red vertical elements and not for green vertical or red horizontal elements.

4) Generalized Double-Opponency (GDO) Mechanisms: Once the signal is processed by the half-square operator, the next task is to extract the texture edge. How will the texture edge be extracted using GDO so as to produce results that are compatible with human performance? Nothdurft's experiments [41] are relevant in this endeavor. His results indicate that edge strength i) improves as the textel density increases and ii) depends on local differences. Thus, a reasonable idea is to perform a local gradient computation of the spatially smoothed (or "pooled") output of the pathways, since the smoothing will produce stronger signals for denser textures. This is equivalent to convolving the outputs with derivatives of smoothing kernels. One possibility is to convolve the image with the second derivative of the Gaussian, G'' (center-surround Laplacian "Mexican hat"). This is shown schematically on the bottom of Fig. 1, which depicts, in one dimension for simplicity, how GDO is implemented for a pair of input signals Q and W to produce the double-opponent output $Q \wedge W$. Double-opponency is produced by convolving Q and W by G'' and $-G''$, respectively, and adding the results. The shape of G'' and the phase difference of 180° ensure that Q and W have an excitatory and inhibitory effect, respectively, in the center of G'' and that their roles reverse in the surround. This construction enables it to have an opponency both within a region and across regions in an image. The classical color double opponent receptive field, as well as the proposed orientation double opponent field, both shown as center-surround Mexican hats are illustrated in Fig. 3. Consider the color double opponent receptive field in Fig. 3: The central portion of the receptive field is excitatory to red and inhibitory to green. However, the surround portion behaves exactly the reverse, i.e., inhibitory to red and excitatory to green. This is a case of chromatic opponency and is present both in the center and surround. The second opponency is of the spatial kind, i.e., red is excitatory in the center and is inhibitory in the surround. The opposite is true for green. The chromatic opponency coupled with the spatial opponency make these units double opponent. Such receptive fields are prevalent in the visual cortex. Looking at such a cell, one can conclude that the best response would be for a stimulus having a red center and a green surround, i.e., a red-green texture edge. Analogously, the best response for our orientation double opponent cells in Fig. 3 would be a stimulus with vertically oriented units in the center and horizontally oriented units in the periphery. Thus such a GDO operation produces a weak signal in regions populated by the same textel types, since the inhibitory and excitatory contributions of each filter tend to cancel each other over space. On the contrary, it produces a strong signal at texture edges, as desired. As a result, the double opponent filters used in the fourth stage of our model are appropriate for detecting texture edges. Such a GDO filter was designed as an isotropic band-pass "Mexican-hat" filter with very low cut-off frequencies. The spatial frequency of the GDO filters were 3 cycles/degree compared to those of the linear filters which were around 12 cycles/degree. As mentioned earlier the spatial frequency of the linear filters

were matched to the size of the individual elements in Fig. 2 which measured 5 arcmin in length and 1.5 arcmin in width. The entire image (one of the 18 stimuli shown in Fig. 4) measured 2° in length and 1° in width.

The next issue is to form the pairs of maps which will be processed by the double-opponency (GDO) operator within each domain [25]. Obviously, within the LnO domain a GDO pair is formed by the A and B pathways (Fig. 1), resulting in the LnO GDO output $a \wedge b$, where the $a \wedge b$ operator is shown at the bottom of Fig. 1, as explained in the beginning of this section. The CnO output is similarly derived in the CnO domain. We next consider the CO domain. Within CO, opponency is obtained in two possible ways: Orientation opponency is obtained by combining the pathways GV with GH to produce $G_{VH} = G_V \wedge G_H$ as well as RV with RH for $R_{VH} = R_V \wedge R_H$. Color opponency within CO is implemented by applying the GDO operator to RV and GV as well as RH and GH to obtain $V_{RG} = R_V \wedge G_V$ and $H_{RG} = R_H \wedge G_H$ respectively. In the LO domain the GDO outputs $A_{VH} = A_V \wedge A_H$ and $B_{VH} = B_V \wedge B_H$ implement orientation opponency, while $V_{AB} = A_V \wedge B_V$ and $H_{AB} = A_H \wedge B_H$ produce polarity opponency. The pairs (GV, RH) and (GH, RV) involve simultaneous opponency in color and orientation and are thus unlikely to be implemented. In essence, one may reasonably argue that a horizontal unit would interact with a vertical unit in the orientation domain and similarly a horizontal-red unit would interact with a horizontal-green unit in the color domain. However, an interaction between a horizontal-red unit with a vertical-green unit would be highly unlikely. We have assigned zero weights for such interactions in our model; psychophysical evidence corroborates this conjecture [25]. The combination of two activity maps Q and W into a single GDO map $M = Q \wedge W$ allows the texture edge to be extracted separately within each GDO map. We used images that contained a vertically oriented texture edge (see Fig. 4). The strength of the edge was estimated by first locating the maximum value of M and then subtracting from it the space-averaged value of E on both sides of the maximum.

5) Combination of Edge Information: After the signals within each pathway are processed by the GDO transformation, the signals must be combined somehow, first within each domain, and then across all domains. This will produce the final activity map from which global texture edges will be extracted. We have selected to use β-summation [61] because it allows the signals to be weighted and summed probabilistically, to account for the degree of independence of the operators. The weights' values will indicate the relative contributions of the different operators in the texture segregation process. To obtain appropriate weights for this combination, we compared the model's responses to results from psychophysical experiments with a carefully chosen set of 18 texture pairs, shown in Fig. 4. We selected those weights which produced the best fit with the psychophysical data. This is explained in detail in Section III-A.

The next task is to combine the outputs within the LO and CO domains, since we have multiple GDO signals in these two domains. Let us consider the CO domain in detail, since the LO domain is quite similar. The edge strengths of orientation-opponent outputs G_{VH} and R_{VH} and the color-opponent outputs H_{RG} and V_{RG} are weighted by K_{OC} and K_C respectively, and combined through β-summation [61] to produce the total signal C_O for the CO domain

$$C_O = \left\{K_{OC}\left[G_{VH}^{\beta} + R_{VH}^{\beta}\right] + K_C\left[V_{RG}^{\beta} + H_{RG}^{\beta}\right]\right\}^{1/\beta}. \quad \text{(1a)}$$

Since K_{OC} and K_C are relative strengths for the two possible mechanisms in the CO domain they can be normalized by requiring that

$$K_{OC} + K_C = 1. \quad \text{(1b)}$$

Similarly, we have

$$L_O = \left\{K_{OL}\left[A_{VH}^{\beta} + B_{VH}^{\beta}\right] + K_L\left[V_{AB}^{\beta} + H_{AB}^{\beta}\right]\right\}^{1/\beta} \quad \text{(2a)}$$

with

$$K_{OL} + K_L = 1. \quad \text{(2b)}$$

The final edge strength F is obtained through β-summation across all four domains with appropriate weights

$$F = \left\{K_{\mathrm{LnO}} L_{\mathrm{nO}}^{\beta} + K_{\mathrm{LO}} L_O^{\beta} + K_{\mathrm{CnO}} C_{\mathrm{nO}}^{\beta} + K_{\mathrm{CO}} C_O^{\beta}\right\}^{1/\beta} \quad \text{(3a)}$$

where weights $K_{\mathrm{LnO}}, K_{\mathrm{LO}}, K_{\mathrm{CnO}}$ and K_{CO} can also be normalized

$$K_{\mathrm{LnO}} + K_{\mathrm{LO}} + K_{\mathrm{CnO}} + K_{\mathrm{CO}} = 1. \quad \text{(3b)}$$

From (1b), (2b), and (3b) it follows that there are five free parameters (degrees of freedom) in the model. The sizes of the linear and GDO filters were held fixed. Strictly speaking, they are also free parameters, but we selected their size to match that of the textels in the images. The value of β was matched to that of the observers, obtained from the slopes of their psychometric curves, i.e., from the plots of % correct as a function of stimulus duration, SD, as explained in Section III-A.

III. Results

In addition to testing our model with data from the psychophysics literature, a variety of other strategic images were selected to test the performance of our model. The entire model was implemented in a highly distributed environment. Ten Sun Sparc 10's sharing the same file system were utilized concurrently to compute efficiently the various filter activity maps of the model. A typical simulation of detecting a texture edge in a 128 × 128 pixel image took about 10 s under normal networking load.

A. Psychophysical Results and Parameter Estimation

We tested the model against the three sets of stimuli of Fig. 4 [25], each consisting of six texture pairs, to investigate the interactions of color, luminance-polarity and orientation in texture segregation. These stimuli are schematized in Fig. 4, with texture elements (textels) composed of elongated bars, characterized by combinations of three attributes: 1) **C**olor (**C**), using only the red and green guns of the monitor; three

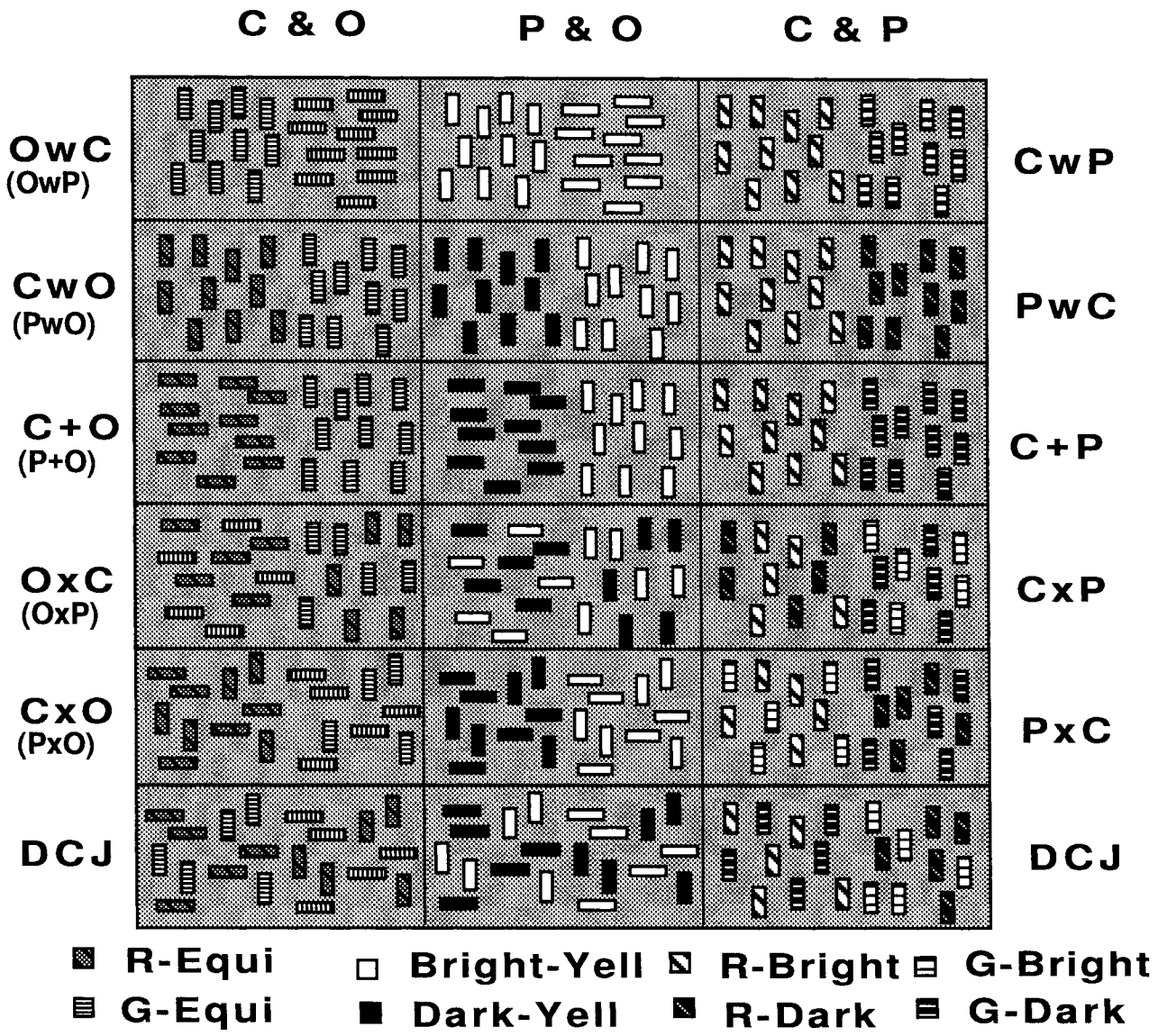

Fig. 4. The 18 texture patterns used in the psychophysical simulations [25] and in model simulations. They are grouped in three sets: Color and Orientation (C & O, left column), Polarity and Orientation (P & O, middle column), and Color and Polarity (C & P, right column) sets. The particular condition within the C & O set is shown on the left margin with parentheses used for the P & O set. The conditions for the C & P set are shown in the right margin.

color values were used: Red ($\mathbf{R}$), green ($\mathbf{G}$) and yellow ($\mathbf{Y}$). 2) **P**olarity ($\mathbf{P}$), using textels above ($\mathbf{A}$), below ($\mathbf{B}$), or equal to ($\mathbf{E}$) the background luminance. 3) **O**rientation ($\mathbf{O}$), with horizontal ($\mathbf{H}$) and vertical ($\mathbf{V}$) bars. In all cases, the background was yellow and its luminance was set at the average luminance of the textels. Texture pairs were organized in three major sets: 1) Set **C&O**, shown on the left panel of Fig. 4: Equiluminant textels defined by $\mathbf{C}$ and $\mathbf{O}$ only, i.e., $\{R \text{ or } G\} \times \{E\} \times \{V \text{ or } H\}$ bars; no luminance signal is present here. 2) Set **P&O** (middle panel): Isochromatic textels defined by $\mathbf{P}$ and $\mathbf{O}$ only, i.e., $\{Y\} \times \{A \text{ or } B\} \times \{V \text{ or } H\}$ bars; there is no chromatic signal in the images of this set. 3) Set **C&P** (right panel): Vertical textels defined by $\mathbf{C}$ and $\mathbf{P}$ only, i.e., $\{R \text{ or } G\} \times \{A \text{ or } B\} \times \{V\}$ bars.

These sets are shown in three columns in Fig. 4. We will use the three-letter notation, generically represented by "CPO," to indicate the values of a textel's color, polarity and orientation, respectively, i.e., GEV denotes a **G**reen, **E**quiluminant (to the background), **V**ertical textel. In the top-most condition of the C & O set, we have GEV textels on the left, GEH on the right. We term this condition O "*within*" C (**OwC**) because segregation is based on O (V versus $\mathbf{H}$), while the color (C) is constant (green) throughout the whole texture. The next entry is the dual condition **CwO**, i.e., segregation due to C, with O fixed. In the $\mathbf{C}+\mathbf{O}$ condition, it is both C and O that achieve segregation. In the condition labeled $\mathbf{O}\times\mathbf{C}$ it is O that achieves segregation, but now the textels' color is not fixed on either side of the edge: we have O *across* C. Dually, in $\mathbf{C}\times\mathbf{O}$, we have segregation based on C, but there are textels of both orientations throughout. Finally, in **DCJ**, we have the *conjunction* of C and O: REH and GEV bars on the left, REV and GEH on the right. Segregation is difficult, because both colors and both orientations are present throughout the image.

Thus, with the exception of DCJ, the trigraphic notation for each condition, such as CwO, has the following symbolic meaning: The first letter of the trigraphic notation denotes the

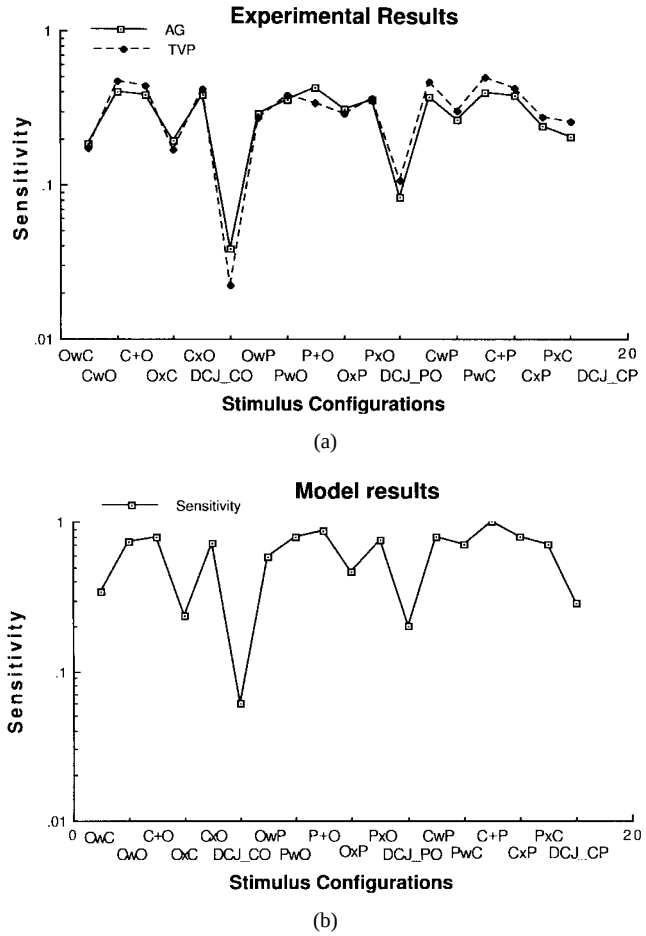

Fig. 5. (a) Psychophysical results from two observers indicating the ease of texture discrimination with the 18 stimuli [25] and (b) model simulations with the same 18 stimuli. Note that the trend of the model simulations is close to that of the psychophysical results.

primary attribute on which discrimination is based, i.e., C or O for the C & O set. The third letter denotes the secondary attribute. The second letter in the trigraph specifies whether the second attribute, is uniform across the two textures to be discriminated [within (w)], varies randomly [across (x)], or covaries positively with the first attribute [plus $(+)$]. For example, the notation OwC (orientation within color) indicates that the texture pair is discriminated on the basis of an orientation difference, while the color is constant within the whole texture. Corresponding texture pairs are formed in sets P & O and C & P. The same notation is used to form mnemonic codes; for example, condition PwO (YAV on the left versus YBV on the right) is labeled P within O, since P varies across the texture edge, while O is fixed. Notice that in the cases involving double conjunction discrimination cannot be based on a single attribute alone (orientation or color), but can be achieved by a conjunction of attributes. The bottom left block in Fig. 4 is an example of double conjunction in the color and orientation domain. Both the left and right sides of the stimulus have red and green elements. Similarly, both sides contain vertical and horizontal elements. However, the left side has only red horizontal units and the right only green horizontal units. Thus this texture can be segmented only with a conjunction of attributes. In other words, the texture boundary is visible, based on orientation differences, if one concentrates on one color, say red; equivalently if one attends to textels of one orientation, say vertical, then the texture edge becomes visible, based on the chromatic difference.

TABLE I
MODEL WEIGHTS

K_{OC}	K_{C}	K_{OL}	K_{L}	K_{CO}	K_{CnO}	K_{LO}	K_{LnO}	β
0.95	.05	.33	.67	.099	.401	.042	.458	2.05

Human performance was measured by asking observers to report the existence of a global texture edge and plotting the percentage of correct responses as a function of SD, the stimulus duration [25]. The value SD* that was necessary to achieve 81.6% correct performance was obtained by fitting the data for each of the 18 conditions to a theoretical psychometric function with a maximum likelihood procedure [25], [61]. Sensitivity was defined as the inverse of the SD*. Results of these experiments are shown in Fig. 5 (top) for two observers. In Fig. 5 sensitivity is plotted as the ordinate, for the 18 conditions, which are shown along the horizontal axis. Solid diamonds and open squares are used for observers TVP and AG, respectively. Results were highly correlated across observers. From the data we observe that the double conjunction textures are hard to discriminate, and have the lowest sensitivities. As a general rule, observers' AG and TVP performances are strongly correlated (Pearson correlations of $r^2 = 0.94$).

We compared the model's performance against the data of Fig. 5(a), and we tried to estimate near-optimal values for the weights of (1b), (2b), and (3b). Strictly speaking, there is a problem comparing the psychophysical data, which are based on temporal factors, to the output of the model, which has no time dependence. However, we assume that the overall edge strength signal, as computed from the model, is monotonically related to the degree to which test texture pairs segregate [26], one measure of which is the sensitivity metric that we obtained in the psychophysical experiments. The weights were adjusted using a simplex optimization search routine in MATLAB [63] to produce as good a fit to the experimental data [25] as possible. The values of the weights are shown in Table I, and were used in all the simulations of this and the next subsection.

The weights, found to correlate with the experimental data, were very robust. A ten percent random variation around the weights shown in the table made less than 0.5% change in the average correlation. The average correlation (across observers and stimulus sets) was 81.5 (Pearson correlation r^2 expressed as a percentage). Fig. 5(b) shows the degree of texture discriminability predicted by our model, when the weights of Table I were used. Note that the trend in the order of discriminability predicted by our model matches the order found experimentally. The average correlation of 81.5 across observers, $(r_{\mathrm{AG}^2} = 80.0, r_{\mathrm{TVP}^2} = 83.0)$ compares favorably with the results of other texture models [Rubenstein and Sagi [48] report 80.0, and Malik and Perona [40] obtain 81.5 (computed from their Table III)]. It should be noted here that our model performs equally well, considering that it has to deal with chromatic images. This correlation figure can be improved further if we transform the model outputs S_E

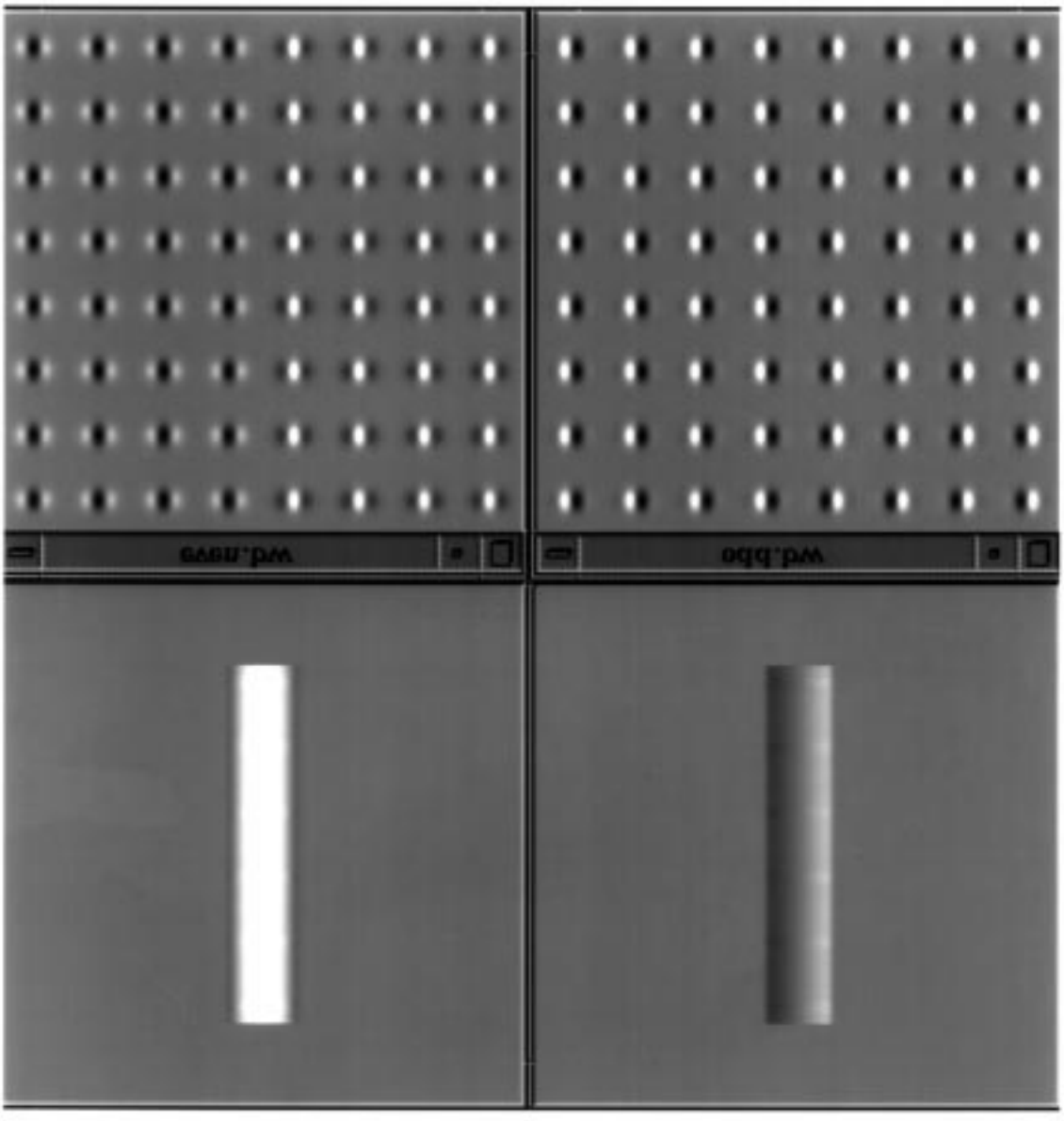

Fig. 6. Even and odd texture stimuli containing textels whose cross-sections are even and odd functions, respectively. Below each stimulus is the response of the texture model. The even texture is easily segregated into two halves by a global vertical edge. However, the top right image (odd case) cannot be easily segregated. These observations are also predicted by our model.

through a monotonic nonlinear function $f(S_E)$, as applied by Graham *et al.* [26], [27].

B. Results With Various Textures

Our model predicts the strong segregation for a texture composed of textels that have a bright center and a dark surround from a texture made up of textels with a dark center and a bright surround ([27, Fig. 1] and [40, Fig. 4]). This example is shown in the top left panel in Fig. 6, and the success of the model can be attributed to the half-squaring operation. It also predicts the weak segregation of an odd antisymmetric texture pair composed of vertical Gabor patches with a single sinusoidal cycle, where one texture contains patches that are bright on the left and the other texture has patches that are dark on the left ([40, Fig. 6]), shown in the right top panel of Fig. 6. It is to be noted that the mean luminance of all four types of textels is the same as the uniform luminance of the background. We consider these two pairs as key tests for any texture model. The top two images in Fig. 6 are the even and odd stimuli, respectively, and below each are the responses of our texture model. Note that there is a much stronger response at the center for the even stimuli (brighter edge corresponds to a stronger response) and a medium response for the odd stimuli.

We also tested our model on a stimulus which has radially directed textels at the center portion of the image and tangential textels at its periphery. This is shown in Fig. 7(a), and it displays a clearly visible circular global texture edge. Such an image can be clearly segregated by our orientation double opponency units which fire for orientation discontinuities in the image. The result is shown in Fig. 7(b). The high activity along the global circular edge is clearly visible, in agreement

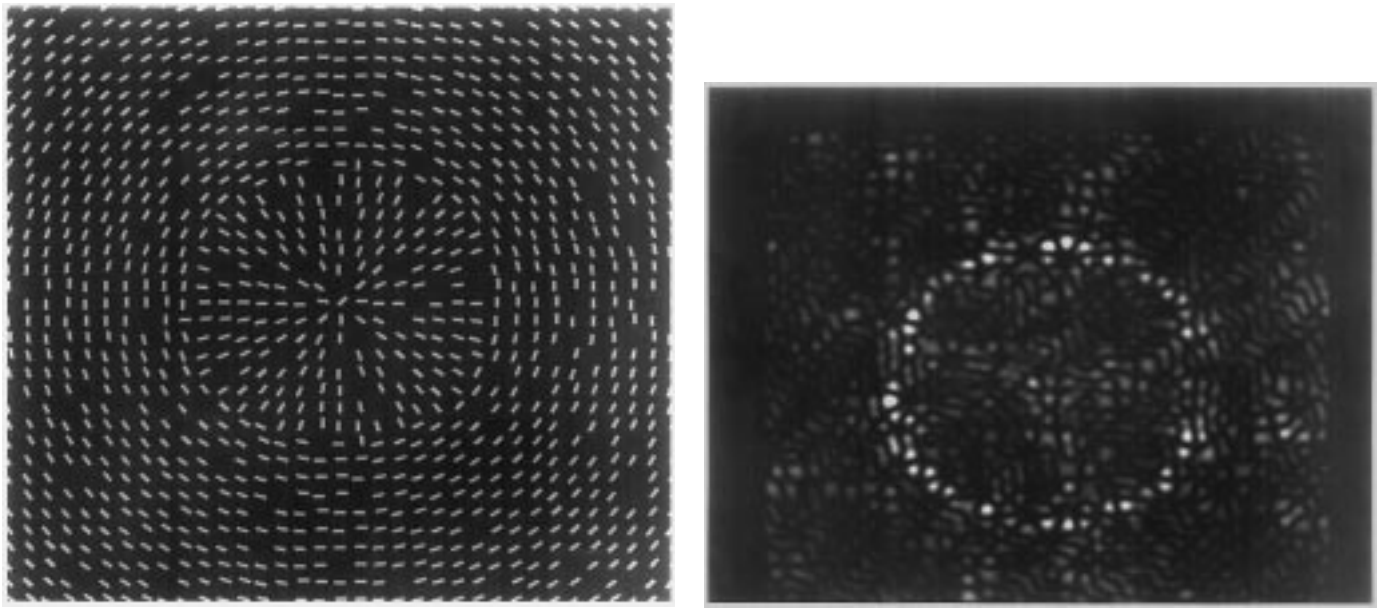

(a) (b)

Fig. 7. (a) The stimulus for an orientation-based texture edge and (b) the result of the model to the stimulus.

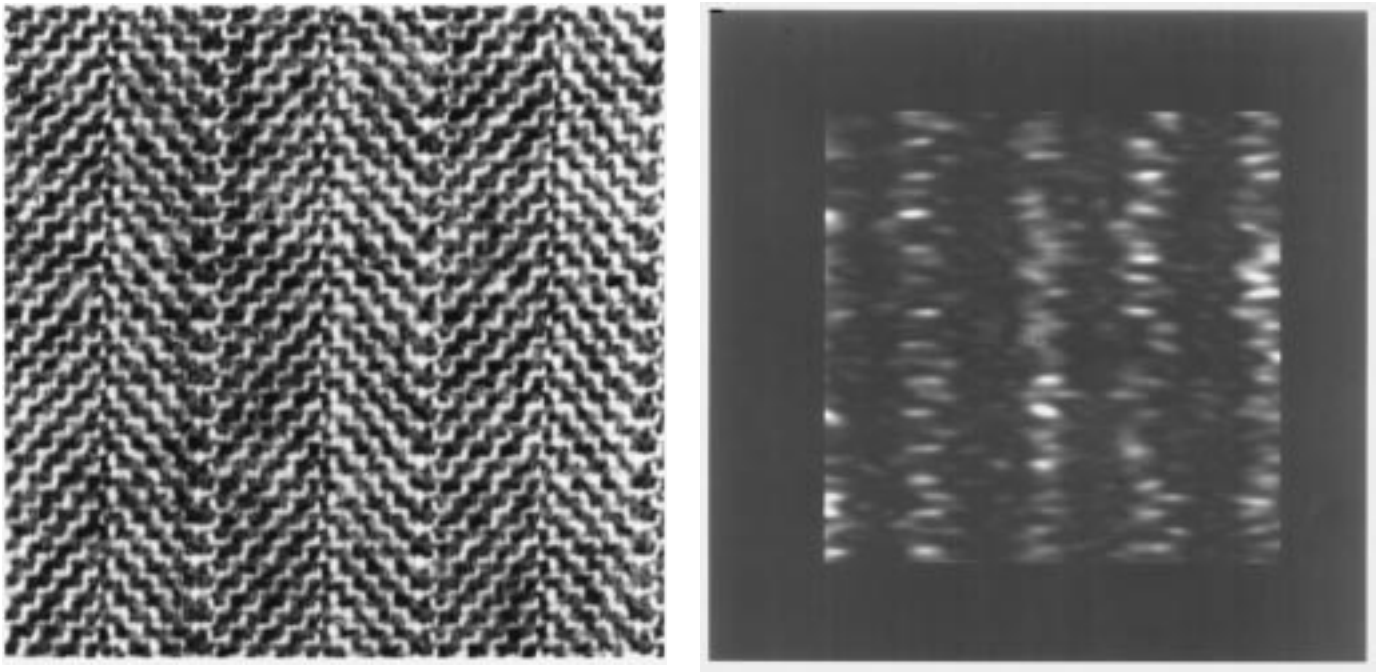

(a) (b)

Fig. 8. An image of a herringbone texture pattern (a) with orientation discontinuities and (b) the model result.

with human performance. This image must also be included as a benchmark test for texture models, since the task here is to segregate a concentric field from a radial one and any model that detects edges within orientation-selective activity maps will encounter difficulties detecting the entire texture edge contour. We also tested our model with natural textures, an example of which (herring-bone pattern) is shown in Fig. 8(a), displaying several discontinuities. We applied this as an input to our model, where the scale of the front end filters was matched to that of the micropatterns of individual threads. The model's result is shown in Fig. 8(b), which clearly shows the texture edges (discontinuities).

IV. Discussion

Edges in images can be broadly classified into two types. The first-order edges are seen in images based solely on differences in retinally available attributes of luminance or color. Such edges are immediately visible to the very early stages of our visual system, i.e., center-surround opponent cells, and they can be termed as "pre-cortical edges." The second-order

edges, or the "cortical edges" are due to derived attributes such as orientation, contrast, spatial frequency, binocular disparity or flicker-rate differences. Essentially our texture model, like many others, transforms the second-order edges to activity maps by convolving the input image with various spatial frequency and orientation tuned filters, which are then put through some nonlinear stages and further smoothed to obtain texture edges. This model illustrates that the concept behind double-opponency can be implemented as a possible mechanism in texture edge extraction. As noticed from the color domain, these double-opponent cells in the cortex fire for red-green edges or blue-yellow edges. An analogous mechanism is detailed in our model to extract orientation edges.

At first glance, our model's orientation opponency is very similar to that of Landy and Bergen [38]. However, there are two important differences: Landy and Bergen's energy units respond strongly to bars of their preferred orientation irrespective of the bars' polarity (this is also true of Fogel and Sagi's model [22]). Our proposed units respond strongly to bars of their preferred orientation only if the bars also match the units' preferred polarity. The second difference is that we incorporate a double-opponency mechanism for orientation, thereby interacting with nearby cells for orientation differences. Such a mechanism would be more effective in extracting orientation contrasts. Thus these double-opponent cells tend to be optimized for seeking texture discontinuities or texture contrasts in a visual field.

There is clear evidence of spatial opponency in attributes other than luminance or color. For example, in the neurophysiology literature, van Essen and his colleagues [37], [58] have recorded from cells in area $V1$ of monkeys with an excitatory surround for orthogonally oriented bars, pointing to orientation opponency, which they believe may play a role in texture segregation. Similar physiological evidence is given by Bonds [10]. In psychophysics, Cannon and Fullenkamp [16] presented evidence of lateral inhibition among mechanisms tuned to different spatial frequencies and orientations by studying how surrounding gratings suppress the contrast of a center grating. Polat and Sagi [45] present evidence of spatial opponency in spatial frequency. Surround patches raise or lower the sensitivity in detecting a patch in the center, depending on whether their spatial frequency is different or the same as that of the center patch.

One approach to finding texture edges is to extract the edge within each activity map using spatial opponency. However, this fails miserably when it comes to comparing cases $O \times C$ and DCJ of our C & O stimuli in Fig. 4; both these stimuli would produce equally strong edges for each of the RV, RH, GV and GH operators of the CO domain. However, we know that DCJ, the conjunction case, is far more difficult than $O \times C$. This is one of the reasons for introducing the concept of generalized double-opponency (GDO) between pairs of activity maps, rather than extracting the edge within each map, and GDO does quite well at predicting the difference in performance.

Another concern of our modeling efforts is the interaction of luminance and chromatic pathways. This can be best understood with our texture stimuli. Consider the double-conjunction of color and polarity (DCJ) (the texture pattern in the bottom right of Fig. 4, in the C & P set). The left half of the field contains red-bright elements and green-dark elements. The right half of the field contains green-bright elements and red-dark elements. The luminance component $L(x, y)$ of this image contains bright and dark elements on both sides of the field, which makes segregation extremely difficult, if not impossible. The chromatic component $C(x, y)$ contains red and green elements on both sides of the field, and this map too does not make it any easier to find a texture edge. Now, if the human visual system did have separate noninteracting luminance and chromatic mechanisms, such a stimulus would not give rise to any texture edge. However, from the experimental data in Fig. 5(a), observers could find a texture boundary in such stimuli. This clearly argues for interacting pathways for color and luminance, and this is the reason for incorporating such an interaction in our model.

The model proposed above is based on the generalization of the concept of double opponency to attributes other than color, such as luminance-polarity and orientation. This is the first successful attempt, to our knowledge, to model human texture segregation performance with textels defined by color, in addition to orientation and luminance (which have been used by other researchers); furthermore, this model has some neurophysiological relevance and its results agree closely with experimental data. However, the limitations of the model must also be noted. First, this model only deals with two opponent mechanisms (i.e., broad-band and red-green), and not with the third one (yellow-blue). The introduction of the third mechanism would allow the model to deal with full-color images. Second, multiple scales must be incorporated to deal with arbitrary inputs automatically, without adjusting the filters' sizes. Third, the issue of asymmetry [49] was not addressed explicitly in this model, but additional psychophysical experiments are necessary to modify the model appropriately.

The model could be utilized in the following areas: a) image processing for the purposes of image segmentation and coding, taking full advantage of the characteristics of the human visual system which, after all, is the "final judge" of image quality and fidelity [44], [57]; b) pattern recognition and machine vision for improving shape-from-texture algorithms which, so far, have been applied to gray-level images [1]; c) scientific visualization for effectively employing visual attributes in order to portray large data sets by coupling them effectively to the human visual system [42]. The model can be extended to other attributes, such as spatial frequency, by constructing GDO operators between adjacent frequency bands that share the same orientation tuning. It remains to be seen whether such GDO units can be isolated in neurophysiological experiments.

REFERENCES

[1] J. Aloimonos, "Shape from texture," *Biol. Cybern.*, vol. 58, pp. 345–360, 1988.
[2] D. Albrecht and D. Hamilton, "Striate cortex of monkey and cat: Contrast response function," *J. Neurophys.*, vol. 48, pp. 217–237, 1982.
[3] J. Beck, "Effect of orientation and of shape similarity on perceptual grouping," *Perception Psychophys.*, vol. 1, pp. 300–302, 1966.
[4] ——, "Textural segmentation," in *Organization and Representation in Perception*, J. Beck, Ed. Hillsdale, NJ: Erlbaum, 1982.
[5] J. Beck, K. Prazdny, and A. Rosenfeld, *Human and Machine Vision*. New York: Academic, 1983.

[6] J. R. Bergen, "Theories of visual texture perception," in *Spatial Vision of Vision and Visual Disfunction*, D. Regan, Ed. New York: Macmillan, vol. 10, pp. 114–134, 1991.

[7] J. R. Bergen and E. H. Adelson, "Visual texture segmentation based on energy measures," *J. Opt. Soc. Amer.*, vol. 3A, p. 98, 1986.

[8] ——, "Early vision and texture perception," *Nature*, vol. 333, pp. 363–364, 1988.

[9] J. R. Bergen and M. S. Landy, "Computational modeling of visual texture segregation," in *Computational Models of Visual Perception*, M. S. Landy and J. A. Movshon, Eds. Cambridge, MA: MIT Press, 1991, pp. 253–271.

[10] A. B. Bonds, "Role of inhibition in the specification of orientation selectivity of cells in the cat striate cortex," *Visual Neurosci.*, vol. 2, pp. 41–55, 1989.

[11] P. Cavanagh, M. Arguin, and A. Treisman, "Effect of surface medium on visual search for orientation and size features," *J. Experimental Psychol.: Human Perception Performance*, vol. 16, pp. 479–491, 1990.

[12] T. Caelli, "On discriminating visual textures and images," *Perception Psychophys.*, vol. 31, pp. 149–159, 1982.

[13] ——, "Three processing characteristics of visual texture segmentation," *Spatial Vision*, vol. 1, pp. 19–30, 1985.

[14] ——, "Texture classification and segmentation algorithms in man and machines," *Spatial Vision*, vol. 7, no. 4, pp. 277–292, 1993.

[15] ——, "A brief overview of texture processing in machine vision," in *Early Vision and Beyond*, T. V. Papathomas, C. Chubb, A. Gorea, and E. Kowler, Eds. Cambridge, MA: MIT Press, 1995, pp. 79–88.

[16] Cannon and Fullenkamp, "Spatial interactions in apparent contrast: Inhibitory effects among grating patterns of different spatial frequencies, spatial positions and orientations," *Vision Res.*, vol. 31, no. 11, pp. 1985–1998, 1991.

[17] C. Chubb and M. S. Landy, "Orthogonal distribution analysis: A new approach to the study of texture perception," in *Computational Models of Visual Perception*, M. S. Landy and J. A. Movshon, Eds. Cambridge, MA: MIT Press, 1991, pp. 253–271.

[18] M. Clark, A. C. Bovik, and W. S. Geisler, "Texture segmentation using a class of narrowband filters," in *Proc. IEEE Int. Conf. Acoustics, Speech, Signal Processing*, 1987.

[19] J. G. Daugman, "Spatial visual channels in the Fourier plane," *Vision Res.*, vol. 24, pp. 891–910, 1984.

[20] R. L. DeValois and K. K. DeValois, *Spatial Vision*. New York: Oxford Univ. Press, 1990.

[21] E. A. DeYoe and D. C. VanEssen, "Concurrent processing streams in monkey visual cortex," *Trends Neurosci.*, vol. 11, pp. 219–226, 1988.

[22] I. Fogel and D. Sagi, "Gabor filters as texture discriminator," *Biol. Cybern.*, vol. 61, pp. 103–113, 1989.

[23] W. T. Freeman and E. H. Adelson, "The design and use of steerable filters," *IEEE Trans. Pattern Anal. Machine Intell.*, vol. 13, pp. 891–906, 1991.

[24] A. Gorea and T. V. Papathomas, "Texture segregation by chromatic and achromatic visual pathways: An analogy with motion processing," *J. Opt. Soc. Amer. A*, vol. 8, no. 2, pp. 386–393, 1991.

[25] ——, "Double-opponency as a generalized concept in texture segregation illustrated with color, luminance and orientation defined stimuli," *J. Opt. Soc. Amer. A*, vol. 10, pp. 1450–1462, 1993.

[26] N. Graham, "Complex channels, early local nonlinearities, and normalization in texture segregation," in *Computational Models of Visual Perception*, M. S. Landy and J. A. Movshon, Eds. Cambridge, MA: MIT Press, 1991, pp. 119–133.

[27] N. Graham, J. Beck, and A. Sutter, "Nonlinear processes in spatial-frequency channel models of perceived texture segregation: Effects of sign and amount of contrast," *Vision Res.*, vol. 32, pp. 719–743, 1992.

[28] S. Grossberg and E. Mingolla, "Neural dynamics of perceptual grouping: Textures, boundaries and emergent segmentations," *Perception Psychophys.*, vol. 38, pp. 141–171, 1985.

[29] L. O. Harvey and M. J. Gervais, "Visual texture perception and Fourier analysis," *Perception Psychophys.*, vol. 24, pp. 534–542, 1978.

[30] D. J. Heeger, "Computational model of cat striate physiology," in *Computational Models of Visual Perception*, M. S. Landy and J. A. Movshon, Eds. Cambridge, MA: MIT Press, 1991, pp. 119–133.

[31] D. H. Hubel and T. N. Wiesel, "Functional architecture of macaque monkey visual cortex," in *Proc. R. Soc. Lond. B*, no. 217, pp. 449–470, 1977.

[32] B. Julesz, "Visual pattern discrimination," *IRE Trans. Informat. Theory*, vol. IT-8, pp. 12–18, 1962.

[33] ——, "Texture and visual perception," *Sci. Amer.*, vol. 212, pp. 38–48, 1965.

[34] ——, "Experiments in perception," *Psychol. Today*, vol. 2, pp. 16–23, 1968.

[35] B. Julesz, E. N. Gilbert, and L. A. Shepp, "Inability of humans to discriminate between visual textures that agree in second-order statistics-revisited," *Perception*, vol. 2, pp. 391–405, 1973.

[36] B. Julesz, E. N. Gilbert, and J. D. Victor, "Visual discrimination of textures with identical third-order statistics," *Biological Cybern.*, vol. 31, pp. 137–140, 1978.

[37] J. J. Knierim and D. C. van Essen, "Neuronal responses to static texture patterns in area V1 of the alert macaque monkey," *J. Neurophysiology*, vol. 67, no. 4, pp. 961–980, 1992.

[38] M. S. Landy and J. R. Bergen, "Texture segregation and orientation gradient," *Vision Res.*, vol. 31, pp. 679–691, 1991.

[39] M. S. Livingstone and D. H. Hubel, "Segregation of form, color, movement and depth: Anatomy, physiology and perception," *Science*, vol. 240, pp. 740–749, 1988.

[40] J. Malik and P. Perona, "Preattentive texture discrimination with early vision mechanisms," *J. Opt. Soc. Amer.*, vol. 7A, pp. 923–932, 1990.

[41] H. C. Nothdurft, "Sensitivity for structure gradient in texture discrimination tasks," *Vision Res.*, vol. 25, pp. 1957–1988, 1985.

[42] T. V. Papathomas, J. A. Schiavone, and B. Julesz, "Application of computer graphics to the visualization of meteorological phenomena," *Comput. Graph.*, vol. 22, pp. 327–334.

[43] T. V. Papathomas and A. Gorea, "Texture segregation with 'double conjunctions' of attributes: A quantitative approach," *Investigative Ophthalmology Visual Sci. Suppl.*, vol. 33, p. 959, 1992.

[44] T. V. Papathomas and D. Malah, "Experimentally obtained thresholds for a conditional replenishment image sequence coder," *J. Visual Commun. Image Represent.*, 1993.

[45] U. Polat and D. Sagi, "Lateral interactions between spatial channels: Suppression facilitation revealed by lateral masking," *Investigative Ophthalmology Visual Sci. Suppl.*, vol. 33, p. 1345, 1992.

[46] W. Richards and A. Polit, "Texture matching," *Kybernetic*, vol. 16, pp. 155–162, 1974.

[47] B. S. Rubenstein, "Image gradients and performance asymmetries in early vision," Ph.D. dissertation, Weizmann Inst. Science, Israel, 1994.

[48] B. S. Rubenstein and D. Sagi, "Spatial variability as a limiting factor in texture-discrimination tasks: Implications and performance," *J. Opt. Soc. Amer.*, vol. 7A, pp. 1632–1643, 1990.

[49] D. Sagi, "The psychophysics of Texture segmentation," in *Early Vision and Beyond*, T. V. Papathomas, C. Chubb, A. Gorea, and E. Kowler, Eds. Cambridge, MA: MIT Press, 1995, pp. 69–78.

[50] R. Shapley, "Visual sensitivity and parallel retinocortical channels," *Annu. Rev. Psychol.*, vol. 41, pp. 635–658, 1990.

[51] G. Sperling, "Three stages and two systems of visual processing," *Spatial Vision*, vol. 4, pp. 183–207, 1989.

[52] A. Sutter, J. Beck, and N. Graham, "Contrast and spatial variables in texture segregation: Testing a simple spatial-frequency channels model," *Perception Psychophys.*, vol. 46, pp. 312–332, 1989.

[53] E. Switkes, A. Bradley, and K. K. DeValois, "Contrast dependence and mechanisms of masking interactions among chromatic and luminance gratings," *J. Opt. Soc. Amer.*, vol. 5A, pp. 1149–1162, 1988.

[54] L. G. Thorell, R. L. DeValois, and D. G. Albrecht, "Spatial mapping of monkey V1 cells with pure color and luminance stimuli," *Vision Res.*, vol. 24, pp. 751–769, 1984.

[55] D. Ts'o, "The functional organization and connectivity of color processing," in *Neural Mechanisms of Visual Perception*, D. M. K. Lam and C. Gilbert, Eds. Woodlands, TX: Portfolio, 1989, pp. 87–115.

[56] M. Turner, "Texture discrimination by Gabor functions," *Biol. Cybern.*, vol. 55, pp. 71–82, 1986.

[57] M. Unser and M. Eden, "Multi-resolution feature extraction and selection for texture segmentation," *IEEE Trans. Pattern Anal. Machine Intell.*, vol. 11, pp. 717–728, 1989.

[58] D. C. van Essen, E. A. DeYoe, J. F. Olavarria, J. J. Krierim, J. M. Fox, D. Sagi, and B. Julesz, "Neural responses to static and moving texture patterns in visual cortex of the macaque monkey," in *Neural Mechanisms of Visual Perception*, D. M. K. Lam and C. Gilbert, Eds. Woodlands, TX: Portfolio, 1990, pp. 137–154.

[59] J. D. Victor, M. M. Conte, K. Purpura, and E. Katz, "Isodipole textures: A window on cortical mechanisms of form processing," in *Early Vision and Beyond*, T. V. Papathomas, C. Chubb, A. Gorea, and E. Kowler, Eds. Cambridge, MA: MIT Press, 1995, pp. 99–108.

[60] H. Voorhees and T. Poggio, "Computing texture boundaries from images," *Nature*, vol. 333, pp. 364–367, 1988.

[61] A. B. Watson, "Probability summation over time," *Vision Res.*, vol. 19, pp. 322–342, 1979.

[62] S. W. Zucker, "Early orientation support: Tangent fields and the dimensionality of their support, *Comput. Vision Graph. Image Process.*, vol. 32, pp. 74–103, 1985.

[63] MATLAB software, MathWorks Inc., Natick, MA.

Thomas V. Papathomas (S'75–M'76) was born in Kastoria, Macedonia, Greece in 1949. He received the B.S., M.S., and Ph.D. degrees from Columbia University, New York, in 1971, 1972, and 1977, respectively, all from the Department of Electrical Engineering and Computer Science.

He was a Member of the Technical Staff in the Electronic Power Systems Laboratory from 1977 to 1982, a supervisor of the AC Control Systems Group from 1982 to 1983, and a Member of the Research Staff in the Visual Perception Research Department from 1983 to 1989, all at AT&T Bell Laboratories, Murray Hill, NJ. Since 1989 he is an Associate Professor in the Department of Biomedical Engineering and the Associate Director of the Laboratory of Vision Research, Rutgers University, Piscataway, NJ. His research interests are in human and machine vision, image processing, imaging systems, and scientific visualization techniques. He has designed several exhibits on stereopsis in science museums, and is the editor-in-chief of *Early Vision and Beyond* (Cambridge, MA: MIT Press, 1995), a volume of interdisciplinary research in psychophysics, neurophysiology, and computational vision.

Dr. Papathomas is a member of Eta Kappa Nu, Tau Beta Pi, Sigma Xi, ACM, OSA (Optical Society of America), SPIE (Society of Photo-Optical Instrumentation Engineers), ARVO (Association for Research in Vision and Ophthalmology), and LIA (Laser Institute of America). Since 1993, he is serving as a member of the editorial board of the *International Journal of Imaging Systems and Technology*.

Ramanujan S. Kashi was born in Bangalore, India, on April 26, 1966. He received the B.E. degree in instrumentation technology from the University of Mysore, India in 1988, and the M.S. and Ph.D. degrees in biomedical engineering from Rutgers University, Piscataway, NJ, in 1991 and 1994, respectively.

Following a year of postdoctoral study funded by the Fight for Sight (research division of Prevent Blindness America) with T. V. Papathomas, at the Laboratory of Vision Research, Rutgers University, he joined Bell Laboratories, Murray Hill, NJ, as a Member of the Technical Staff. His research interests are in human and computational vision, visual perception and pattern recognition problems as related to handwriting recognition.

Dr. Kashi is a member of ARVO (Association for Research in Vision and Ophthalmology).

Andrei Gorea was born in 1952 in Bucharest, Romania. He received the Master of clinical psychology degree and the Diploma of the ''Ecole Pratique des Hautes Etudes'' in experimental psychology, both from Paris VII University, France, in 1975. He received the Ph.D. degree in experimental psychology and the ''These d'Etar'' in neurosciences from the Rene Descartes University, Paris, in 1978 and 1986, respectively.

He has been with the National Center for Scientific Research (CNRS), Paris, France, since 1978 and is now Director of Research. He is also an Adjunct Associate Professor at the Pierre and Marie Curie University and Rene Descartes University. His scientific experience mainly covers the psychophysics of spatio-temporal aspects of vision perception, motion perception, grouping and segregation of moving and textured multi-attribute stimuli, dynamic stereo, 3-D from 2-D stimuli and bistable perception, and visual attention. He was an Associate Editor of *Spatial Vision* and organizer of the 13th ''European Conference on Visual Research'' (ECVP) in Paris, 1990.

Dr. Gorea is a member of the Optical Society of America (OSA), the European Brain and Behavior Society (EBBS), and Association for Research in Vision and Ophthalmology (ARVO).